Pergamon

Chemical Engineering Science, Vol. 51, No. 19, pp. 4477–4488, 1996

0009-2509/96 $15.00 + 0.00

PII: S0009-2509(96)00291-6

EFFECT OF VISCOSITY ON RETENTION TIME AND HYDRODYNAMIC LIFT FORCES IN SEDIMENTATION/STERIC FIELD-FLOW FRACTIONATION

P. STEPHEN WILLIAMS, MYEONG HEE MOON,† YUEHONG XU and J. CALVIN GIDDINGS*

Field-Flow Fractionation Research Center, Department of Chemistry, University of Utah, Salt Lake City, UT 84112, U.S.A.

(*Received* 27 *March* 1995; *accepted* 26 *February* 1996)

Abstract—Particles entrained in fluid flow between parallel bounding walls tend to be driven by hydrodynamic forces, acting perpendicular to the direction of flow, towards certain equilibrium positions between the walls. Sedimentation field-flow fractionation is a technique that is well suited to the measurement of these forces, particularly in the regions close to the walls. Forces much stronger than those due to fluid inertial effects are commonly observed in the near-wall regions. A study is presented here of the influence of carrier fluid viscosity on these hydrodynamic lift forces. The carrier viscosity is varied via two different methods: (1) various ternary mixtures of water, glycerol, and ethanol were used that varied in viscosity while being of constant density and (2) the temperature of the FFF system was raised, changing the carrier viscosity while not significantly altering its density. The near-wall lift forces are shown to be dependent on fluid viscosity. An empirical equation describing the apparent dependence is presented.

Keywords: Field-flow fractionation, hydrodynamic lift force, viscosity.

INTRODUCTION

Sedimentation/steric field-flow fractionation (Sd/StFFF), a subtechnique of field-flow fractionation that was first developed over 15 years ago (Giddings and Myers, 1978), has in recent years become a powerful technique for particle separations and particle size analysis (Koch and Giddings, 1986; Giddings *et al.*, 1991; Williams *et al.*, 1992b; Giddings and Moon, 1991; Moon and Giddings, 1992, 1993). This FFF subtechnique is capable of fully resolving particles differing in diameter by no more than 15–20% over the size range from 0.3 to 60 μm (see Fig. 1). The separation time is now typically 3 min but can be as short as 1 min or as long as 10 min. Thus particle size analysis by Sd/StFFF is relatively fast and is characterized by a much higher resolving power than provided by light scattering techniques. Furthermore, unlike any other high-speed automatable technique, narrow size fractions can be readily collected from the eluting stream and subjected to microscopic or other forms of examination to correlate particle morphology, extent of aggregation, or particle composition with size and to confirm, if desired, that the particle size provided by calibration is correct. In addition, Sd/StFFF can be used to measure the density and porosity of near-spherical particles (Giddings and Moon, 1991).

An essential step in carrying out particle size analysis by Sd/StFFF is that of establishing a relationship between retention time and particle diameter. This relationship is used to convert the detector response vs time curve (the fractogram) to a particle size distribution curve. For submicron-sized particle analysis, the retention time–diameter relationship can be established on the basis of theory (see, for example, Giddings, 1978, 1984, 1988, 1993; Caldwell, 1988). Thus no calibration is necessary to obtain a particle size distribution. However, in Sd/StFFF calibration is necessary because a component of the underlying forces governing retention, namely hydrodynamic lift forces, are not well understood and not accounted for by traditional inertial lift force theory (Williams *et al.*, 1992a, b, 1994). While the calibration procedure usually employs polystyrene latex standards and is not particularly onerous, in some cases calibration must be done based on the size measurement of fractions of more dense particles by microscopic examination. Particle size analysis by Sd/StFFF could be further streamlined if these calibration steps could be avoided. To do so requires a clearer understanding of hydrodynamic lift forces, which in turn requires a broader base of experimental data. The technique of Sd/StFFF in fact provides a versatile methodology for the experimental study of the underlying lift forces (Williams *et al.*, 1992a, 1994), and will be used here to further evaluate lift force effects.

The earlier study (Williams *et al.*, 1992a), in which over 500 retention measurements were made for polystyrene latex beads of different diameters that were subjected to different external forces (perpendicular to the flow vectors) under different shear conditions, revealed that inertial lift effects were unable to

* Corresponding author.
† Current address: Department of Chemistry, Kangnung National University, Kangnung, Kangwon-Do, Korea, 210–702.

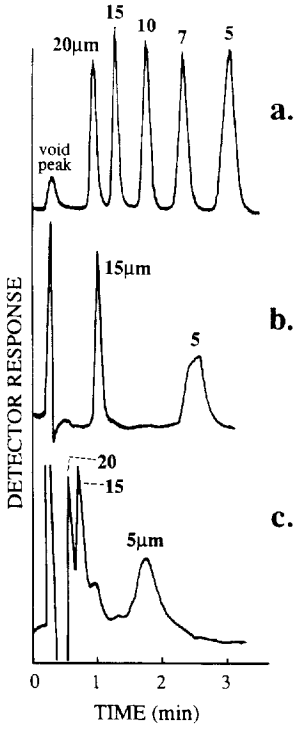

Fig. 1. Fractograms demonstrating high resolution separation of polystyrene standards obtained at 1300 rpm and flow rate $\dot{V}$ = 6.01 ml/min. Carrier liquid viscosities for the three runs were (a) 0.933, (b) 2.65, and (c) 4.93 cP.

account for the lift forces near the wall of the FFF channel. The dominating lift force F_{Lw} for particles near the wall appeared to be governed by the equation

$$F_{Lw} = C\frac{a^3 s_0}{\delta} \tag{1}$$

where C is a constant, a the particle radius, s_0 the undisturbed fluid shear rate at the wall, and δ the distance of closest approach between the particle and the wall. Equation (1) is distinctly different from that based on inertial effects, the latter involving a lift force proportional to the square of s_0 and the fourth power of a. In the more recent work (Williams *et al.*, 1994), involving particles driven both close to the wall and more distant (several radii) from the wall, it was found that the measured lift force could be described as the sum of a contribution given by eq. (1) and a contribution due to fluid inertial effects (see later).

Equation (1), with its first-order dependence on s_0, suggests that the near-wall lift forces originate in viscous effects, perhaps related to lubrication phenomena. If so, the constant C should be proportional to viscosity and indeed has the dimensions of viscosity. However, according to very general hydrodynamic arguments, first-order forces [such as described by eq. (1)] perpendicular to a plane wall should not exist. A puzzling aspect of this argument is that it appears to rule out major aspects of lubrication phenomena in which load-bearing surfaces are held apart by a thin viscous film of liquid.

The purpose of this work is to use Sd/StFFF to extend our previous studies of near-wall lift forces by examining specifically the effects of variations in liquid viscosity. This study was carried out using two different approaches. For the first approach the carrier solution was composed of ternary water–glycerol–ethanol mixtures. Five different compositions were used such that the viscosity varied over a five-fold range while the density was held constant to within 0.3%. For the second approach the temperature of the system was varied in step-wise fashion from 25°C to 70°C. Over this range the viscosity of the aqueous carrier changes more than two-fold while the density changes only by 2%. Thus using both methods we were able to independently measure the effects of viscosity without large concomitant changes in liquid density which would influence inertial lift effects.

THEORY

Mechanism of steric mode retention

For the initial, simplistic model of particle retention in steric FFF (Giddings and Myers, 1978), particles were assumed to be driven to the so-called accumulation wall under the influence of the applied field and there swept along the channel by the flow of carrier. The particles were assumed to remain in close proximity to the wall during migration and their velocity to correspond to the undisturbed fluid velocity at the location of their centers. Within the typical thin, parallel-walled FFF channel the carrier fluid velocity is well described by the parabolic equation

$$v(x) = 6\langle v\rangle \frac{x}{w}\left(1 - \frac{x}{w}\right) \tag{2}$$

where $v(x)$ is the velocity at a distance x from one wall (by convention, the accumulation wall), $\langle v\rangle$ is the mean fluid velocity, and w is the channel thickness. The retention ratio R, defined as the ratio of the retention time of a non-retained tracer material (i.e. the void time t^0) to that of the retained particles t_r, is then given by

$$R = \frac{t^0}{t_r} = \frac{v_p}{\langle v\rangle} = 6\alpha(1 - \alpha) \tag{3}$$

where v_p is the particle velocity and $\alpha = a/w$. For $a \ll w$, eq. (3) reduces to the very simple form

$$R = 6\alpha. \tag{4}$$

In practice, however, the action of hydrodynamic lift forces tends to drive the particles away from the accumulation wall. In addition, the velocity of a particle entrained in a sheared flow bounded by a wall is predicted to be less than that of undisturbed fluid at the position of the particle center (Goldman *et al.*, 1967). (This phenomenon was referred to as the *particle retardation effect* in our previous publications.) Retention time is therefore not generally well predicted by the simple model. Following observation of

what was at first considered to be anomalous retention (Giddings *et al.*, 1979; Caldwell *et al.*, 1979), a dimensionless steric correction factor γ was included in the expression for retention ratio, so that

$$R = 6\gamma\alpha. \tag{5}$$

The steric correction factor γ is generally of order unity and has been found to increase with the flow velocity and to decrease with the increase of field strength (Giddings *et al.*, 1979; Caldwell *et al.*, 1979). These variations in γ have since been interpreted in terms of an interplay between the hydrodynamic lift and sedimentation forces acting on the particle, together with the position dependent correction to particle velocity. Provided the particle shear Reynolds number Re_s($= sa^2\rho/\eta$, where s is the local undisturbed fluid shear rate) is small in comparison to unity, the degree of retardation is predicted to be a function only of the ratio of the distance δ($= x - a$) between the particle and the wall to the particle radius (Goldman *et al.*, 1967). Retardation is therefore independent of fluid properties. The particle velocity when the particle center lies at some arbitrary distance x from the accumulation wall is then given by

$$v_p = f\left(\frac{\delta}{a}\right) v(x) = 6f\left(\frac{\delta}{a}\right)\langle v\rangle \frac{x}{w}\left(1 - \frac{x}{w}\right) \tag{6}$$

where $f(\delta/a)$ is the retardation factor. A method for obtaining $f(\delta/a)$ for any value of δ/a has been presented previously (Williams *et al.*, 1992a). By combining eqs (3) and (6), the retention ratio for migration at position x is obtained as

$$R = 6f\left(\frac{\delta}{a}\right)\frac{x}{w}\left(1 - \frac{x}{w}\right). \tag{7}$$

When a sample pulse is introduced into the flowing carrier at the channel inlet, the particles are driven towards their equilibrium distances from the accumulation wall under the influence of the opposed sedimentation and lift forces while at the same time being swept along the axis of the channel. If the time characterizing the migration to an equilibrium position (the relaxation time) is small compared to the overall retention time, then the apparent R (measured as t^0/t_r) will differ little from the equilibrium value. In this case, eq. (7) may be solved numerically for equilibrium δ and x values given the particle size and channel thickness. Generally a correction must be applied to the apparent R to obtain an estimate to the equilibrium R. The required correction is derived later.

Determination of near-wall lift force

At the point of equilibrium, the sedimentation force F_G on a particle will exactly counter the lift force F_L, the latter being considered to be the sum of fluid inertial and near-wall contributions as explained earlier. At equilibrium then

$$|F_G| = F_L = F_{Li} + F_{Lw} \tag{8}$$

where F_{Li} represents the inertial contribution and F_{Lw} the near-wall contribution to lift force. Since F_G is precisely known, rather exact F_L values can be obtained. The inertial contribution is given by (Cox and Brenner, 1968; Ho and Leal, 1974; Vasseur and Cox, 1976; Cox and Hsu, 1977; Williams *et al.*, 1994)

$$F_{Li} = 13.5\,\frac{\pi a^4 \langle v\rangle^2 \rho}{w^2}\, g\left(\frac{x}{w}\right) \tag{9}$$

where ρ is the density of the carrier and $g(x/w)$ is a function given approximately by

$$g\left(\frac{x}{w}\right) = 19.85\left(0.19 - \frac{x}{w}\right)\left(0.5 - \frac{x}{w}\right)\left(0.81 - \frac{x}{w}\right). \tag{10}$$

An improved, fifth-order approximation for $g(x/w)$ is given by (Williams, 1994)

$$g\left(\frac{x}{w}\right) = 19.85\left(0.19 - \frac{x}{w}\right)\left(0.5 - \frac{x}{w}\right)\left(0.81 - \frac{x}{w}\right) \times\left[1 + \frac{16}{12}\frac{x}{w}\left(1 - \frac{x}{w}\right)\right]. \tag{11}$$

This approximation was assumed for the present work.

The derivation of the above equations for F_{Li} is valid within certain constraints. For example, the particle must be negligibly small relative to the channel thickness (i.e. $a \ll w$), and it must not closely approach either wall (i.e. $a \ll x$ and $a \ll w - x$). The effects of relaxing the second constraint have recently been examined by Cherukat and McLaughlin (1994). Their results suggest that as the ratio of x/a decreases the inertial lift force is at first enhanced slightly in comparison with F_{Li} as given by eqs (9) and (11). For the region of x/a from ~ 5 to ~ 3 the enhancement approaches $\sim 10\%$. However, this enhancement is predicted to diminish with closer approach of x/a to unity. We shall ignore this relatively small effect in the present work.

Once the equilibrium position of the particle is established through the measurement of t_r and thus of the apparent R [by solution of eq. (7) for the relaxation corrected R], the strength of the inertial lift force may be calculated. For any given experimental conditions, the sedimentation force $|F_G|$ on the particle is also known, being given by

$$|F_G| = \frac{4}{3}\pi a^3 G\Delta\rho \tag{12}$$

in which $\Delta\rho$ is the density difference between particle and fluid and G is the centrifugal acceleration equal to $\omega^2 r_0$, in which ω is the angular velocity of the centrifuge and r_0 is the radius of the channel. In the interest of simplicity, $\Delta\rho$ is assumed to be positive in this treatment so that the resultant F_G is negative (i.e. towards the accumulation wall) and is opposed by a positive lift force. The excess lift force, equal to F_{Lw}, is then obtained by subtracting F_{Li} from $|F_G|$. A series of retention time measurements for particle standards

eluted under various conditions may thereby be used to generate a data set of F_{Lw} with independent variables a, s_0, δ, and η.

Relaxation correction for R

There are two strategies for dealing with the problem of relaxation. Procedures may be utilized to minimize relaxation time, or a correction may be applied to apparent retention ratios to account for the relaxation process. A method of minimizing the relaxation time is to introduce the sample to the channel inlet and then stop the channel flow for a period of time (called the stop-flow time) sufficient for the particles to be driven to the accumulation wall under the influence of the applied field. When the flow is restarted the particles have only a relatively short distance (of order δ) to migrate to their equilibrium positions, being driven from the wall by hydrodynamic lift forces. This method was employed in our earlier studies of lift forces (Williams *et al.*, 1992a, 1994). In the more recent work (Williams *et al.*, 1994), a numerical procedure was included in the data treatment to account for the residual perturbation to the retention ratio. In the present work this stopped-flow method was not used; the so-called stopless-flow method was employed in which the particles are allowed to relax under normal flow conditions. An approximate correction to apparent R for this type of sample introduction may be derived as follows.

A relaxation correction to R for the case of sample particles of negligible size was presented previously (Hovingh *et al.*, 1970; Lee *et al.*, 1989). This approach is modified here to take finite particle size and steric migration into account by adapting the *core channel* concept (Giddings, 1978) to our needs. It is necessary to make some simplifying assumptions, however. As a particle is removed from the vicinity of the walls, the strong near-wall lift force contribution and the particle retardation effect attenuate quickly. The predicted influence of the walls on the particle friction factor for perpendicular motion (Maude, 1961; Brenner, 1961) also rapidly attenuates. These effects may therefore be ignored without incurring significant error. In the central region of the channel only the inertial force will generally be of significance. Due to the symmetry of this force, however, we can expect there to be some cancellation of its effect on the migration of a particle along the length of the channel as it falls from the upper wall to the accumulation wall. For example, in the region from $x/w = 0.81$ to 0.5, the inertial lift force opposes the sedimentation force; the particle falls more slowly, and is swept further along the channel than it would in the absence of lift. In the region from $x/w = 0.5$ to 0.19 the inertial lift acts in the direction of the sedimentation force. The particle consequently falls more quickly and migration along the channel length is therefore reduced. Similarly, the effects of inertial lift force on migration in the regions of $x/w > 0.81$ and < 0.19 will partially cancel. For simplicity, the influence of the inertial lift force will also be ignored.

The core channel, in its original conception (Giddings, 1978), represented the region within the channel accessible to the center of a particle. It excluded those regions within a particle radius of the walls, and therefore had a thickness of $w - 2a$, or $w(1 - 2\alpha)$. Here we shall assume that the core has a thickness $w - 2x_{eq}$, where x_{eq} is the equilibrium value of x, and that this differs little from $w - 2a$. However, instead of the core moving relative to the channel walls at a velocity of $6\langle v\rangle\alpha(1 - \alpha)$, we shall assume it moves at the velocity $R_{eq}\langle v\rangle$, where R_{eq} is the equilibrium value for R. Given the stated assumptions, the time τ_c for relaxation across the full thickness of the core is then given by

$$\tau_c = \frac{w}{|U|}(1 - 2\alpha) \tag{13}$$

where $|U|$ is the sedimentation velocity in the unbounded carrier liquid. During relaxation a particle will migrate a distance h_{0c} within the core, given by

$$h_{0c} = \tau_c\langle v_c\rangle = \frac{\langle v\rangle w}{|U|}(1 - 2\alpha)^3 \tag{14}$$

where $\langle v_c\rangle = \langle v\rangle(1 - 2\alpha)^2$ is the mean flow velocity within the core relative to the (moving) boundaries of the core region.

For a sample that is initially uniformly distributed across the thickness of the channel core, the center of gravity of the band will migrate a distance of $h_{0c}/2$ in the time τ_c. During this same period the core moves a distance $R_{eq}\langle v\rangle\tau_c$ relative to the channel walls. Therefore, the center of gravity advances a total distance $z(\tau_c)$ in ime τ_c where

$$z(\tau_c) = \frac{\langle v\rangle w}{2|U|}(1 - 2\alpha)^3 + R_{eq}\frac{\langle v\rangle w}{|U|}(1 - 2\alpha). \tag{15}$$

Once a particle has relaxed to its equilibrium position it will migrate at the velocity $R_{eq}\langle v\rangle$. The band center of gravity must migrate the remaining distance of $L - z(\tau_c)$ at this velocity, where L is the channel length. The total time of elution t_r is therefore given by

$$t_r = \tau_c + \frac{L - z(\tau_c)}{R_{eq}\langle v\rangle}. \tag{16}$$

Substituting for τ_c and $z(\tau_c)$ this reduces to

$$t_r = \frac{L}{R_{eq}\langle v\rangle} - \frac{w(1 - 2\alpha)^3}{2R_{eq}|U|}. \tag{17}$$

The ratio $L/\langle v\rangle$ is equal to the void time t^0, and thus eq. (17) may be rearranged to

$$\frac{1}{R_{app}} = \frac{1}{R_{eq}}\left\{1 - \frac{\langle v\rangle w}{2L|U|}(1 - 2\alpha)^3\right\}$$

$$= \frac{1}{R_{eq}}\left\{1 - \frac{h_{0c}}{2L}\right\} \tag{18}$$

where $R_{app} = t^0/t_r$ is the apparent retention ratio. Substituting for $|U|$ using Stokes' law, and rearranging we obtain the final expression

$$R_{eq} = R_{app}\left\{1 - \frac{9\eta w(1-2\alpha)^3}{4a^2 G\Delta\rho t^0}\right\}. \quad (19)$$

The use of Stokes' law for the sedimentation velocity across the core channel thickness requires particle Reynolds numbers for the sedimentation velocity Re_{sed} ($= d|U|\rho/\eta$) to be small compared to unity. For example, equations tabulated by Clift *et al.* (1978) suggest that the Stokes law sedimentation velocity would be in error by less than 2% at $Re_{sed} = 0.1$, by about 7% at $Re_{sed} = 0.5$, and by 13% at $Re_{sed} = 1$. For the experiments reported below, it is only for the case of the largest particle size sedimenting under the highest field strength within the lowest viscosity carrier fluid that Re_{sed} approaches unity. However, for these conditions the corrections to retention ratio as given by eq. (19) are negligible. Those conditions for which eq. (19) provides a significant correction for retention ratio in fact correspond to $Re_{sed} \ll 1$, and we can therefore assume the calculated correction to be reasonable.

EXPERIMENTAL

The sedimentation FFF system used in this study has the same basic structure as the model S101 Colloid/Particle Fractionator from FFFractionation, Inc. (Salt Lake City, UT). The channel accumulation wall was constructed of polished Hastelloy-C alloy, and was not coated or treated in any way. The channel has a breadth b of approximately 1 cm, a tip-to-tip length L_{tt} of 90 cm (equivalent to rectangular length L of 88 cm), and a radius r_0 within the centrifuge basket of 15.1 cm. The channel spacer material, from which the channel volume was cut and removed, was Mylar of nominal thickness 0.0127 cm. (This particular batch of Mylar was known to be undersized.) On completion of both sets of experiments, a direct measurement of the assembled channel thickness and of its components indicated a mean channel thickness of close to 0.0112 cm. The breadth of the channel outline was measured at several points along the length and a mean of 1.01 cm was obtained. Some uncertainty remains in b since this can change on positioning the spacer between the two walls. The void volume V^0 was calculated to be 0.995 ml (assuming $b = 1.01$ cm). The void volume was also indirectly determined as a measure of the retention volume for the non-retained peak for sodium benzoate. This method resulted in $V^0 = 1.18$ ml, excluding the total dead volume (0.44 ml) of the tubes leading from the injection point to the channel and then out to the detector. The discrepancy is substantial, and this uncertainty in V^0 must be taken into account when assessing the results of the data treatment. Between the ternary carrier study and the elevated temperature study, the channel was disassembled for cleaning. The direct, geometrical measurement approach was not applied before disassembly, but sodium benzoate elution suggested a V^0 of 1.18 ml, as later observed. Nevertheless, channel thickness could have differed slightly for the two sets of experiments.

The particle standards used in this study were polystyrene-divinyl benzene copolymer latex beads (Duke Scientific, Palo Alto, CA) of density 1.05 g/ml and with nominal diameters of 20.49, 15, 9.87, 7.04, and 5.002 μm (hereafter referred to as 20, 15, 10, 7, and 5 μm, respectively). All experiments were carried out using the stopless flow injection method. The pulse of latex beads was injected, generally as a mixture of sizes, directly into the carrier flow at the channel inlet using a microsyringe and septum injector while the centrifuge was spinning at the required rate.

Carrier fluid was driven by a Kontron LC pump (Kontron Electrolab, London, U.K.) for flow rates less than 10 ml/min, and by an FMI Lab pump model QD-2 (Fluid Metering, Inc., Oysterbay, NY) for higher channel flow rates, and also for flushing the channel at relatively high speed (about 30 ml/min). The eluted sample was monitored at 300 nm by a Spectroflow Monitor SF770 (Kratos Analytical Instruments, Westwood, NJ) UV-VIS detector. A strip chart recorder (Houston Instrument Corp., Austin, TX) was used for recording the response.

As mentioned earlier, the carrier viscosity was varied in two different ways. In the first set of experiments, the carrier was composed of ternary mixtures of glycerol, ethanol, and water; their proportions were chosen to maintain almost constant density while increasing viscosity relative to that of water. In all cases, 0.1% (v/v) FL-70 detergent (Fisher Scientific, Fair Lawn, NJ) was added for dispersion of particles, and 0.02% (w/v) sodium azide was added as a bactericide. The volume fractions of glycerol and ethanol for the different carrier compositions are listed in Table 1 together with their measured viscosities and densities. Viscosities were measured using a Cannon–Ubbelohde Viscometer (Cannon Instrument Co., State College, PA) and densities using a pycnometer obtained from Kimble Glass Co., Vineland, NJ. All measurements and experiments were carried out at an ambient temperature of 296.0 ± 0.5 K. Carrier flow rates $\dot{V}$ of 3.02, 4.45, 6.01, 8.45, and 12.8 ml/min and centrifuge rotation rates of 900, 1300, and 1800 rpm were used. A total of 243 measurements of R were made in this set.

Table 1. Volume fractions of glycerol and ethanol in ternary carrier liquids together with their measured viscosities and densities at 296 K

Glycerol	Ethanol	Viscosity (cP)	Density (g/ml)
0.000	0.000	0.933	0.998
0.060	0.120	1.72	0.999
0.120	0.240	2.65	1.000
0.180	0.360	3.93	0.998
0.245	0.440	4.93	0.999

Table 2. Temperatures used for aqueous carrier study with corresponding viscosities and densities.

Temperature (K)	Viscosity (cP)	Density (g/ml)
343	0.404	0.978
328	0.504	0.986
313	0.653	0.992
298	0.890	0.997

For the second set of experiments the carrier was doubly distilled, deionized water, again with 0.1% (v/v) FL-70 and 0.02% (w/v) sodium azide added. Carrier viscosity was reduced by raising the temperature of the system above ambient. The modifications to the FFF instrument for temperature elevation have been described previously (Giddings *et al.*, 1994). A tape heater was attached to the inside of the rotor shield and the entire channel system was thermally isolated. The carrier reservoir was heated to ~ 15 K above the channel temperature to reduce the amount of dissolved gas and minimize formation of bubbles within the channel. A bubble trap, heated to about the temperature of the reservoir, was placed close to the channel inlet. The temperatures used, together with the corresponding densities and viscosities, are listed in Table 2. For these experiments, the carrier flow rate $\dot{V}$ was fixed at 5.68 ml/min, the centrifuge was set at rotation rates of 900, 1200, 1500, and 1800 rpm, and 62 measurements of R were made. The two sets of experiments had in common a subset using an aqueous carrier at ambient temperature.

It was mentioned earlier that in order for the function $f(\delta/a)$ of Goldman *et al.* (1967) to be valid the particle shear Reynolds number Re_s must be small compared to unity. The local undisturbed shear rate is of course a function of the particle equilibrium position but the shear rate at the channel wall provides an upper bound for this quantity. For the range of experimental conditions considered it may be shown that Re_s approaches unity only for the largest particles in aqueous carrier solution, either at room temperature with the highest $\dot{V}$ of 12.8 ml/min, or at the highest temperature with $\dot{V} = 5.68$ ml/min. Values of Re_s for other particle sizes and conditions were considerably less than unity. Conditions consistent with finite Re_s are of course required to induce hydrodynamic lift.

RESULTS AND DISCUSSION

Typical fractograms for polystyrene latex standards, shown in Fig. 1, were obtained with the three different carrier viscosities of 0.933, 2.65, and 4.93 cP. All three runs were made at 1300 rpm with the carrier flow rate $\dot{V} = 6.01$ ml/min. It is evident that retention time decreases with increase of carrier viscosity. The overall lift force must therefore increase with increase of viscosity. An increased lift force tends to drive particles towards higher equilibrium positions above the accumulation wall. In these higher positions they encounter faster carrier velocities which sweep them through the channel in shorter times. Since the inertial lift force is independent of carrier viscosity, the increase in overall lift must be accounted for by an increase in the near-wall lift contribution.

For the carrier viscosity of 2.65 cP, only the 15 and 5 μm standards were eluted. The others were found to be adsorbed on the Hastelloy-C channel wall by microscopic examination of the surface. It was apparent that the adsorbed particles were aggregated with those of like size. The aggregates may have a greater chance of physical contact with the wall due to their irregular and/or extended shapes and be more likely to be adsorbed than non-aggregated particles. The tendency to aggregate and/or adsorb is likely to be dependent on surface charge density and this may vary for the different particle sizes. When the carrier viscosity is increased further to 4.93 cP, a better recovery of the sample peaks was obtained. This may be explained in terms of a smaller chance of aggregation due to decreased interparticle movement in the more viscous carrier. The presence of a stronger near-wall lift force may also be a factor.

It is noted that band broadening increases in the elution of 5 μm particles with high viscosity carriers (in runs *b* and *c* in Fig. 1). Since the sample is introduced to the channel by stopless flow injection while the channel is spinning, the transverse velocity $|U|$ of particles across the channel (driven by the sedimentation force) will be lower with the more viscous carriers. Thus the initial sample zone will be broadened to a greater degree as the particles pass through the various streamlines of the parabolic flow, i.e. h_{0c} will be larger as predicted by eq. (14).

It has been pointed out (Williams *et al.*, 1994) that the functional form of the empirical equation found to describe near-wall lift force is strongly influenced by the functional form of the velocity slip function $f(\delta/a)$. Reasons for accepting the validity of the slip function as described by Goldman *et al.* (1967) were discussed at length. However, it is possible to examine the dependence of total lift force on carrier viscosity without the assumption of any specific functional form for $f(\delta/a)$ as long as such a function is known to exist. In this case, the elution of a given particle size at some arbitrary equilibrium retention ratio occurs at a fixed x/w and therefore at a fixed value of $f(\delta/a)$ [see eq. (7)] no matter what the viscosity. If, for fixed $\dot{V}$, retention ratios are measured as a function of field strength G for different values of the carrier viscosity η, then interpolation between data points to any particular level of retention will yield a G vs η relationship. Since the lift force is equal to the acceleration force F_G [see eq. (8)], the sought after dependence of F_L is provided. One method of carrying out this procedure is illustrated in Fig. 2. In Fig. 2(a) the data collected for the 15 μm diameter particles with ternary carrier at $\dot{V} = 6.01$ ml/min are plotted in the form of $\log(R_{eq})$ vs $\log(F_L)$, R_{eq} having been obtained from the measured R_{app} using eq. (19). [The data presented in Fig. 2 were adjusted for an assumed w of 0.0117 cm, this being the

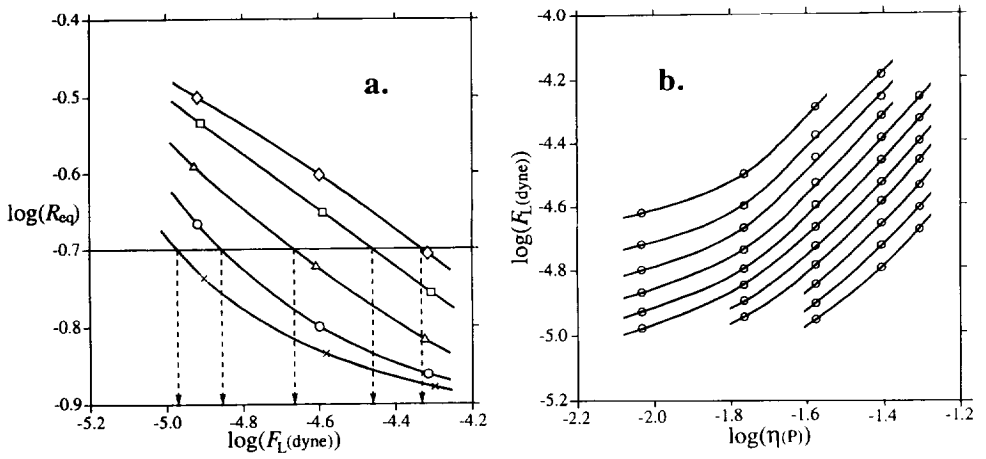

Fig. 2. (a) Retention data for 15 μm particles eluted using each of the five ternary carriers at $\dot{V} = 6.01$ ml/min plotted in the form of $\log(R_{eq})$ versus $\log(F_L)$ (R_{eq} increases with increase of η), and (b) interpolated $\log(F_L)$ plotted against $\log(\eta)$ for retention levels corresponding to $\log(R_{eq})$ from -0.775 to -0.525, at intervals of 0.025.

value required for consistency between data sets as shown later. Adjustment of w was assumed to directly influence V^0, so that both R_{app} and $\langle v \rangle$ were appropriately modified, together with w, α and t^0 of eq. (19).] It is assumed that the R_{eq} so obtained is equal to the true equilibrium retention ratio, so that $F_L = |F_G|$. Smooth curves are drawn through the data points corresponding to each carrier viscosity used. The interpolations to obtain $\log(F_L)$ for each η are shown in Fig. 2(a) for a fixed retention level corresponding to $\log(R_{eq}) = -0.70$. In Fig. 2(b) the interpolated $\log(F_L)$ values are plotted against $\log(\eta)$ for retention levels corresponding to $\log(R_{eq})$ from -0.825 to -0.575 at intervals of 0.025.

Figure 2(b) demonstrates that F_L varies with η for all levels of retention considered. We know that the inertial lift force does not contribute to this observed variation [see eq. (9)], and therefore all variation must be attributed to the additional contribution F_{Lw}. Again, smooth curves are drawn through the points corresponding to each R_{eq}. For each of the curves there is a different constant F_{Li} contribution to the overall F_L. At low viscosities the contribution due to F_{Lw} will be relatively small, and the slope of the curve, representing the power dependence of F_L on η, will be correspondingly small, approaching zero as the viscosity dependent F_{Lw} contribution approaches zero. Conversely, at high viscosities F_{Lw} must dominate and the slope will approach the power dependence of F_{Lw} on η. The curves appearing in Fig. 2(b) indicate that F_L varies with η raised to the power ~ 1.3 in the region of highest viscosity considered. The results shown in Fig. 2 are typical for the various particle sizes and flow rates used.

It is not possible to deduce via this approach the true power dependence of F_{Lw} on η across the range of η considered. The behavior at low η is masked by the η-independent F_{Li} contribution to overall F_L. The inertial contribution may, in some cases, be significant even at the highest η considered here. In these cases, the dependence of F_{Lw} on η would be underestimated at all η by assuming it corresponded with that of F_L. The dependence of F_{Lw} on η may be determined only if we accept the validity of the $f(\delta/a)$ function. The procedure is explained below.

If we assume that $f(\delta/a)$ is known correctly for all δ/a, R_{eq} for each datum may be substituted into eq. (7) and the equation solved numerically for δ_{eq} and x_{eq} ($= a + \delta_{eq}$). In each case the F_{Li} contribution may then be calculated using eqs (9) and (11), and this subtracted from $|F_G|$ [given by eq. (12)] to yield F_{Lw}. The data are thereby transformed to a set of F_{Lw} with independent variables a, s_0, δ, and η. The power dependencies of F_{Lw} on a, s_0, and δ may be obtained for each η via multiple linear regression of $\log(F_{Lw})$ to $\log(a)$, $\log(s_0)$, and $\log(\delta)$. Initially the data for both sets of experiments were adjusted for an assumed w of 0.0112 cm. The results of the described data treatment are listed in Table 3. Compared to our previous studies, the power dependencies of 3, 1, and -1 for a, s_0, and δ, respectively, are not so clearly indicated. The ternary carrier work suggests a dependence of F_{Lw} on a^3, but a less than linear proportionality with both s_0 and $1/\delta$. On the other hand, the elevated temperature work suggests a slightly greater dependence on δ than simply inverse, with the dependence increasing with decreasing η. There tends to be some correlation between η and δ for the data collected (this is a natural consequence of measuring retention ratios over the same range of field strength for each of the carrier viscosities), so an increasing dependence of F_{Lw} on δ with decreasing δ cannot be discounted. A possible explanation for this apparent increasing dependence is given later where the effects of surface roughness are considered. Also listed in Table 3 are the best fit constants of proportionality C_1 (with units corresponding to viscosity in P) obtained on forcing integer powers consistent with eq. (1).

Table 3. Power dependencies of F_{Lw} on a, s_0, and δ found by multiple linear regression

	Power dependencies					
η(cP)	a	s_0	δ	$C_1 \times 10^5$ (P)	$C_2 \times 10^5$ (P)	$C_3 \times 10^5$ (P)
Elevated temperature study. Assumed w = 112 μm						
0.404	2.35	—	− 1.59	0.975	1.17	0.984
0.504	2.39	—	− 1.46	1.06	1.22	1.06
0.653	2.50	—	− 1.31	1.13	1.29	1.13
0.890	2.59	—	− 1.15	1.44	1.59	1.44
Ternary carrier study. Assumed w = 112 μm						
0.933	2.80	0.463	− 0.699	0.514	0.597	0.550
1.72	3.09	0.612	− 0.735	1.08	1.08	1.19
2.65	3.22	0.773	− 0.697	2.58	2.54	3.02
3.93	3.19	0.409	− 0.694	6.06	9.08	8.10
4.93	3.06	0.502	− 0.581	11.9	17.5	16.1
Ternary carrier study. Assumed w = 117 μm						
0.933	2.89	0.479	− 0.652	1.33	1.44	1.48
1.72	3.14	0.623	− 0.689	2.62	2.53	2.94
2.65	3.29	0.742	− 0.656	6.07	5.64	6.84
3.93	3.33	0.788	− 0.632	14.0	17.9	15.9
4.93	3.21	0.788	− 0.560	24.3	31.6	29.0

C_1 is the constant of proportionality obtained on forcing integer power dependencies. C_2 and C_3 are the constants of proportionality for least squares regression of predicted F_L and predicted R, respectively.

If we accept the power dependencies of F_{Lw} on a, s_0, and δ as given by eq. (1) across the range of η, we may use alternative regression methods in which the sum of the squares of either the relative errors in predicted F_L or in predicted retention ratios are minimized. The best fit constants of proportionality C_2 and C_3, respectively, are also listed in Table 3. The values obtained for C_1, C_2, and C_3 are generally comparable for each η, and they follow essentially the same trend of increasing with increase of η.

No matter which method of regression we consider, there appears to be a discontinuity in C between the two data sets. It is known, however (Williams *et al.*, 1994), that the magnitude of best fit C is highly sensitive to the assumed channel thickness. As mentioned earlier, the channel was disassembled for cleaning between the two sets of experiments. Both the channel breadth and thickness could have changed slightly on reassembly. It is a relatively simple matter to recalculate the results for the ternary carrier experiments for various assumed channel thicknesses. The coefficient resulting from least squares regression of predicted retention ratio was selected for determination of consistency, since the retention ratio is the primary measurement made in these experiments. Consistency between data sets (i.e. elimination of discontinuity in C_3) was achieved for $w = 0.0117$ cm for the ternary carrier experiments and $w = 0.0112$ cm for the elevated temperature experiments. The combined results are plotted as log(C) vs η in Fig. 3 with the best linear fit given by

$$\log(C) = -5.134 + 33.53\eta \qquad (20)$$

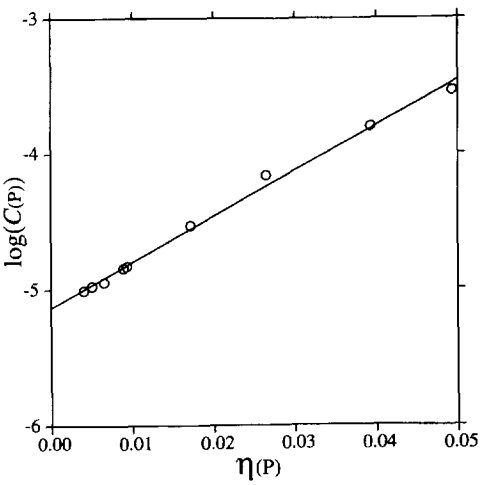

Fig. 3. Plot of log(C) versus η obtained by least squares regression of predicted R with assumed w of 117 μm for the ternary carrier experiments and 112 μm for the elevated temperature experiments. The best linear fit [eq. (20)] is included.

which may be transformed to

$$C = 7.349 \times 10^{-6} \exp(77.21\eta). \qquad (21)$$

Numerical coefficients are consistent with dimensions of P for both C and η. We chose this form of plot solely for the apparent linearity which best discloses any discontinuity. A slightly better, third-order polynomial fit to the data is shown in Fig. 4. This is given by

$$C = 5.072 \times 10^{-6} + 9.863 \times 10^{-4}\eta - 7.069 \times 10^{-3}\eta^2 + 2.110\eta^3. \qquad (22)$$

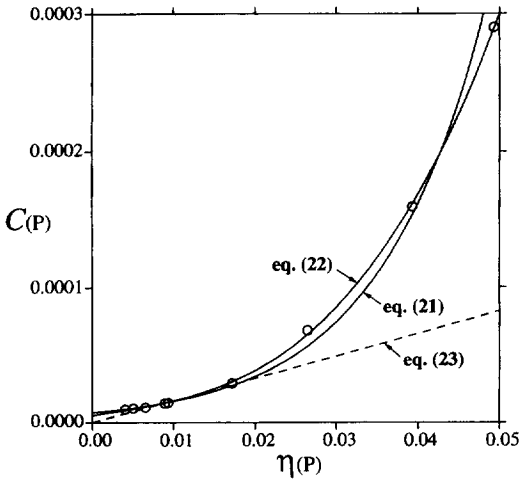

Fig. 4. Plot of C vs η obtained by least squares regression of predicted R with assumed w of 117 μm for the ternary carrier experiments and 112 μm for the elevated temperature experiments. The best third-order polynomial fit [eq. (22)] is shown along with the best exponential fit [eq. (21)] and a linear fit through the datum at $\eta = 0.933$ cP [eq. (23)].

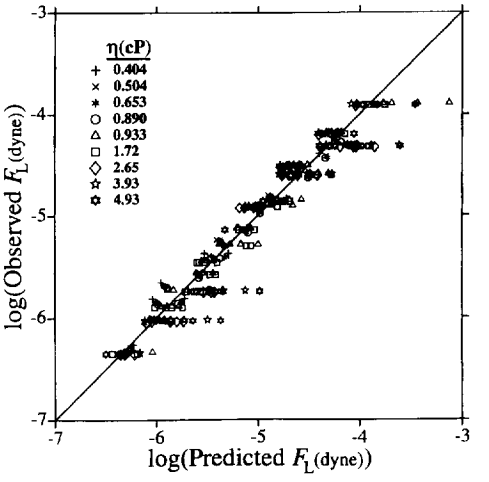

Fig. 5. Logarithmic plot of observed F_L vs predicted F_L, where the latter is given by eq. (8) with F_{Li} given by eqs (9) and (11) and F_{Lw} by eqs (1) and (22).

Equation (21) is plotted together with eq. (22) for comparison in Fig. 4.

It has been stated (Williams *et al.*, 1992) that preliminary work had suggested the possibility of a linear relationship between F_{Lw} and η. The dashed straight line also shown in Fig. 4 represents such a relationship where it is assumed that C is correctly determined for $\eta = 0.00933$ P. The assumption that C at $\eta = 0.00933$ P is given by eq. (22) results in

$$C = 0.00165\,\eta \qquad (23)$$

in which the numerical coefficient is dimensionless. The linear relationship is seen in Fig. 4 to be quite reasonable over a limited range of η. Equation (23) differs from eq. (22) by less than 10% from $\eta = 0.0063$ to 0.018 P. Experiments performed over a wider range of η, as reported here, show an apparent inadequacy of the simple linear relationship. For $\eta < 0.0042$ P and $\eta > 0.024$ P, F_{Lw} is found to be underestimated by eq. (23) by more than 25%. At $\eta = 0.034$ P, F_{Lw} is twice as great as predicted by eq. (23).

A previous study (Williams *et al.*, 1994) was carried out at $\eta = 0.00933$ P. System materials, including channel walls, particles, and carrier composition, were identical to those used in the present study for this viscosity. A dimensionless coefficient was determined for F_{Lw} (where linear dependence of F_{Lw} on η was assumed) which is directly comparable to the numerical coefficient of eq. (23) above. The coefficient previously found varied from 0.00472 to 0.00960 depending on whether a channel thickness of 127 or 132 μm was assumed. Given the uncertainty in w and the sensitivity of C to assumed w, the magnitude of F_{Lw} at $\eta = 0.00933$ P agrees quite well with that found in the present study.

At the low η extreme, the discrepancy between experiment and eq. (23) may be attributable to the effects of channel wall and/or particle surface roughness. When a particle is forced to migrate very close to a wall, as is the case for many of the low-η experiments, any surface roughness is likely to allow easier passage of fluid between particle and wall than would be found for the model system consisting of a perfectly spherical particle and an absolutely flat wall. Thus retardation would be less than predicted by $f(\delta/a)$. The solution of eq. (7) would then yield erroneously high values for x_{eq} and δ_{eq}. These errors would in turn lead to overestimation of F_{Lw}, and hence C, for small δ and therefore also for small η (due to the correlation between δ and η in the experiments). Surface roughness could also directly influence the path of a particle, where periodic contact or near-contact momentarily forces the particle into faster streamlines. Alternatively, at small δ, lift due to repulsive electrostatic or electrokinetic effects may become dominant. Certainly, if we are to attribute F_{Lw} directly to some viscous effect, we must expect F_{Lw} and C to approach zero as η approaches zero.

Figure 5 shows a logarithmic plot of observed F_L vs predicted F_L, in which the symbols represent the various carrier viscosities. The predicted F_L is given by $F_{Li} + F_{Lw}$, where F_{Li} is given by eqs (9) and (11) and F_{Lw} by eqs (1) and (22). Most of the outliers are seen to correspond to the most viscous carriers. Lift forces for the experiments cover a range of almost three orders of magnitude, and are generally predicted by our empirical equations to an accuracy such that $|\log(\text{Observed } F_L) - \log(\text{Predicted } F_L)| < \sim 0.2$. The observed R_{app} data (i.e. the experimentally measured R) are plotted vs predicted R_{app} in Fig. 6 where again the symbols represent the different carrier viscosities. There appears to be a tendency to underestimate R for $R > 0.3$. This may be due to increased error in our approximate relaxation correction in this region. The

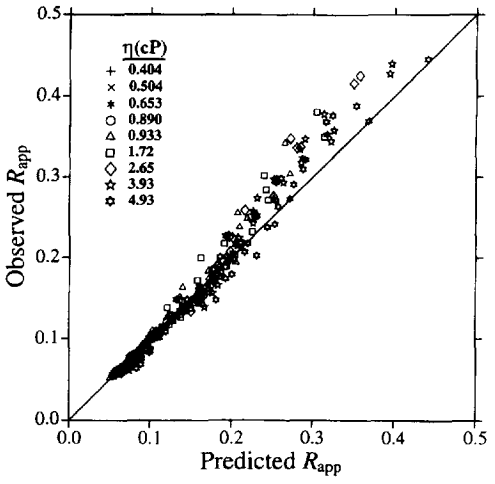

Fig. 6. Plot of observed R_{app} (experimental R) versus predicted R_{app}.

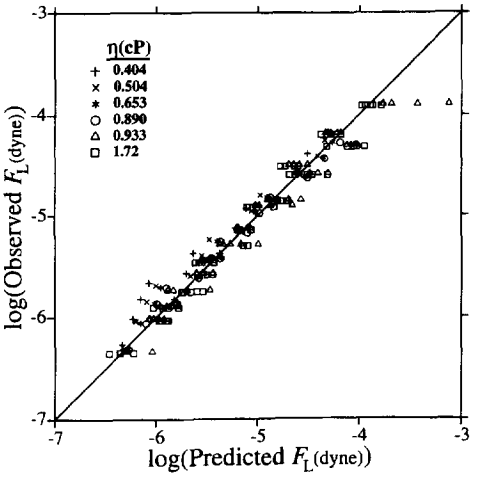

Fig. 8. Logarithmic plot of observed F_L vs predicted F_L, where the latter is given by eq. (8) with F_{Li} given by eqs (9) and (11) and F_{Lw} by eqs (1) and (23). Only data for $\eta \leqslant 1.72$ cP are included.

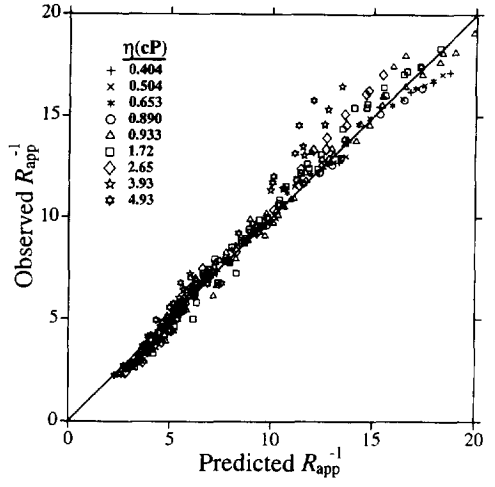

Fig. 7. The data of Fig. 6 plotted in reciprocal form.

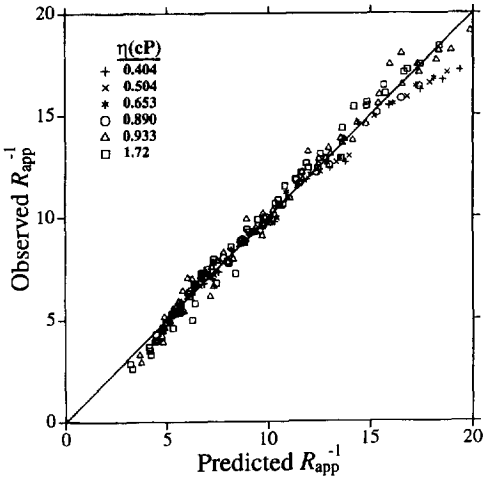

Fig. 9. Plot of observed R_{app}^{-1} vs predicted R_{app}^{-1} for data corresponding to $\eta \leqslant 1.72$ cP with F_L given as in Fig. 8.

viscosity and particle size tend to be high in this region. The correction increases with η [see eq. (19)], but is inversely proportional to a^2. However, the lift forces and the influence of the channel walls on particle friction coefficient [both of which were ignored in the derivation of eq. (19)] are greatest for large a. Another possibility is that inertial lift forces are underestimated for $R > 0.3$. For particles eluting at relatively high R, the inertial lift force tends to dominate. The theory leading to F_{Li} as given by eqs (9) and (11) requires that $a \ll w$, a requirement that may not be sufficiently fulfilled for the larger particles, and as mentioned earlier, finite particle size is expected to result in slightly increased F_{Li} (Cherukat and McLaughlin, 1994). On the other hand, the relative magnitude of F_{Li} may be increased by assumption of a slightly reduced w (this is because $F_{Li} \propto \langle v \rangle^2$, whereas $F_{Lw} \propto \langle v \rangle$). The data of Fig. 6 are plotted in reciprocal form in Fig. 7. Since $t_r \propto 1/R$, this figure gives a better idea of how well we can predict retention times via our empirical lift force equations.

It was shown earlier that a linear dependence of F_{Lw} on η [consistent with eq. (23)] is acceptable for a limited range of η. Figure 8 shows a logarithmic plot of observed F_L vs predicted F_L [where F_{Lw} is given by eqs (1) and (23)] for all data corresponding to $\eta \leqslant 0.0172$ P. A comparison of this plot with that shown in Fig. 5 shows that F_L is indeed quite well predicted for these conditions. The reciprocals of observed R_{app} are plotted vs predicted values for these same conditions in Fig. 9. The agreement is very good over the full range of retention. Specifically, the root mean square deviation of the $1/R_{app}$ points (and thus retention time values) from the correlation line is 6.3%.

CONCLUSION

The reported experiments provide strong evidence that a component of hydrodynamic lift force in parallel plate systems has a dependency on the fluid viscosity. As in our previously reported studies, this component has been shown to be quite well described by the empirical relationship given by eq. (1). A total of more than 1100 measurements of retention time in sedimentation/steric FFF have thus far been shown to support this empirical description. We have also demonstrated that for carrier viscosities that do not exceed ~0.02 P, this component of lift force is quite well described by the equation

$$F_{Lw} = C' \frac{a^3 \eta s_0}{\delta} \tag{24}$$

where C' is a dimensionless coefficient. For higher viscosities, the measured force is greater than predicted by eq. (24).

As our capability for predicting lift forces improves, so does our ability to relate retention time to particle diameter under well controlled laboratory conditions. The prospect of obtaining accurate particle size data (without calibration) improves simultaneously. However, lift forces are still not sufficiently well known for particle size calculations, with the largest uncertainties arising with any attempt to transfer lift force correlations from one experimental system to another.

Clearly, further work is indicated. With the continuing improvements being made in FFF instrumentation, the precision of retention time measurements is also sure to improve. The precise determination of channel void volume and instrument dead volumes has been shown to be of primary importance for determining absolute strength of the hydrodynamic forces being measured.

Acknowledgement—This work was supported by Grant CHE-9322472 from the National Science Foundation.

NOTATION

a	particle radius
b	breadth of channel
C	coefficient of the empirical near-wall lift force as given by eq. (1)
d	particle diameter
$f(\delta/a)$	particle retardation factor
F_G	sedimentation force
F_L	lift force
F_{Li}	inertial lift force
F_{Lw}	near-wall lift force
$g(x/w)$	function of x/w given by eq. (10)
G	field strength measured as acceleration
G_1	effective field strength at unit viscosity
h_{0c}	distance migrated along core channel by particle sedimenting across core thickness
L	equivalent rectangular channel length
L_{tt}	tip-to-tip channel length
r_0	radius of rotation of sedimentation channel
R	retention ratio
R_{app}	apparent retention ratio
R_{eq}	equilibrium retention ratio
Re_p	particle Reynolds number
Re_s	particle shear Reynolds number ($= sa^2\rho/\eta$)
Re_{sed}	particle sedimentation Reynolds number
s	local undisturbed shear rate
s_0	undisturbed shear rate at the wall
t_r	retention time
t^0	void time
$\|U\|$	sedimentation velocity
$v(x)$	carrier velocity at distance x from accumulation wall
v_p	particle velocity along length of channel
$\langle v \rangle$	mean carrier velocity
$\langle v_c \rangle$	mean carrier velocity within core channel
$\dot{V}$	volumetric carrier flow rate
x	distance of particle center from the accumulation wall
x_{eq}	equilibrium distance of particle center from the accumulation wall
w	channel thickness
$z(\tau_c)$	distance migrated along channel by particle relaxing across thickness in time τ_c

Greek letters

α	ratio of a to w
γ	steric correction factor
δ	distance from particle surface to the wall, equal to $x - a$
δ_{eq}	equilibrium distance from particle surface to the wall, equal to $x_{eq} - a$
$\Delta\rho$	density difference between particle and the carrier fluid
η	carrier viscosity
ρ	density of carrier fluid
τ_c	relaxation time for particle in core channel
ω	angular velocity of centrifuge

REFERENCES

Brenner, H., 1961, The slow motion of a sphere through a viscous fluid towards a plane surface, *Chem. Engng. Sci.* **16**, 242–251.

Caldwell, K. D., 1988, Field-flow fractionation, *Analyt. Chem.* **60**, 959A–971A.

Caldwell, K. D., Nguyen, T. T., Myers, M. N. and Giddings, J. C., 1979, Observations on anomalous retention in steric field-flow fractionation, *Separat. Sci. Technol.* **14**, 935–946.

Cherukat, P. and McLaughlin, J. B., 1994, The inertial lift on a rigid sphere in a linear shear flow field near a flat wall, *J. Fluid Mech.* **263**, 1–18.

Clift, R., Grace, J. R. and Weber, M. E., 1978, *Bubbles, Drops, and Particles*, Chap. 5, p. 112. Academic Press, New York.

Cox, R. G. and Brenner, H., 1968, The lateral migration of solid particles in Poiseuille flow – 1. Theory, *Chem. Engng. Sci.* **23**, 147–173.

Cox, R. G. and Hsu, S. K., 1977, The lateral migration of solid particles in a laminar flow near a plane, *Int. J. Multiphase Flow* **3**, 201–222.

Giddings, J. C., 1978, Displacement and dispersion of particles of finite size in flow channels with lateral forces. Field-flow fractionation and hydrodynamic chromatography, *Separat. Sci. Technol.* **13**, 241–254.

Giddings, J. C., 1984, Field-flow fractionation, *Separat. Sci. Technol.* **19**, 831–847.

Giddings, J. C., 1988, Field-flow fractionation, *C&E News* (10 October) **66**, 34–45.

Giddings, J. C., 1993, Field-flow fractionation: separation and characterization of macromolecular, colloidal, and particulate materials, *Science* **260**, 1456–1465.

Giddings, J. C., Moon, M. H., Williams, P. S. and Myers, M. N., 1991, Particle size distribution by sedimentation/steric FFF: development of a calibration procedure based on density compensation, *Analyt. Chem.* **63**, 1366–1372.

Giddings, J. C. and Moon, M. H., 1991, Measurement of particle density, porosity, and size distributions by sedimentation/steric field-flow fractionation: application to chromatographic supports, *Analyt. Chem.* **63**, 2869–2877.

Giddings, J. C. and Myers, M. N., 1978, Steric field-flow fractionation: a new method for separating 1–100 μm particles, *Separat. Sci. Technol.* **13**, 637–645.

Giddings, J. C., Myers, M. N., Caldwell, K. D. and Pav, J. W., 1979, Steric field-flow fractionation as a tool for the size characterization of chromatographic supports, *J. Chromat.* **185**, 261–271.

Giddings, J. C., Xu, Y. and Myers, M. N., 1994, Enhancement of performance in sedimentation field-flow fractionation by temperature elevation, *Analyt. Chem.* **66**, 3047–3053.

Goldman, A. J., Cox, R. G. and Brenner, H., 1967, Slow viscous motion of a sphere parallel to a plane wall. II. Couette flow. *Chem. Engng. Sci.* **22**, 653–660.

Ho, B. P. and Leal, L. G., 1974, Inertial migration of rigid spheres in two-dimensional unidirectional flows, *J. Fluid Mech.* **65**, 365–400.

Hovingh, M. E., Thompson, G. H. and Giddings, J. C., 1970, Column parameters in thermal field-flow fractionation, *Analyt. Chem.* **42**, 195–203.

Koch, T. and Giddings, J. C., 1986, High-speed separation of large (> 1 μm) particles by steric field-flow fractionation, *Analyt. Chem.* **58**, 994–997.

Lee, S., Myers, M. N. and Giddings, J. C., 1989, Hydrodynamic relaxation using stopless flow injection in split inlet sedimentation field-flow fractionation, *Analyt. Chem.* **61**, 2439–2444.

Maude, A. D., 1961, End effects in a falling-sphere viscometer, *Br. J. Appl. Phys.* **12**, 293–295.

Moon, M. H. and Giddings, J. C., 1992, Extension of sedimentation/steric field-flow fractionation into submicron range: size analysis of 0.2–15 μm metal particles, *Analyt. Chem.* **64**, 3029–3037.

Moon, M. H. and Giddings, J. C., 1993, Rapid separation and measurement of particle size distribution of starch granules by sedimentation/steric field-flow fractionation, *J. Food Sci.* **58**, 1166–1171.

Vasseur, P. and Cox, R. G., 1976, The lateral migration of a spherical particle in two-dimensional shear flows, *J. Fluid Mech.* **78**, 385–413.

Williams, P. S., 1994, Particle trajectories in field-flow fractionation and SPLITT fractionation channels, *Separat. Sci. Technol.* **29**, 11–45.

Williams, P. S., Koch, T. and Giddings, J. C., 1992a, Characterization of near-wall hydrodynamic lift forces using sedimentation field-flow fractionation, *Chem. Engng Commun.* **111**, 121–147.

Williams, P. S., Moon, M. H. and Giddings, J. C., 1992b, Fast separation and characterization of micron size particles by sedimentation/steric field-flow fractionation: role of lift forces. In *Particle Size Analysis*, (Edited by Stanley-Wood, N. G. and Lines, R. W.), pp. 280–289. Royal Society of Chemistry, Cambridge, UK.

Williams, P. S., Lee, S. and Giddings, J. C., 1994, Characterization of hydrodynamic lift forces by field-flow fractionation: inertial and near-wall lift forces, *Chem. Engng Commun.* **130**, 143–166.